Supplementary Information

Highly Efficient Visible-Light Photocatalytic Ethane Oxidation into Ethyl Hydroperoxide as a Radical Reservoir

Yao Zhu,[a,†] Siyuan Fang,[b,†] Shaoqin Chen,[a] Youjie Tong,[a] Chunling Wang,[a]* and Yun Hang Hu[b]*

a. School of Environmental Science and Engineering, Shanghai Jiao Tong University, Shanghai 200240, China

b. Department of Materials Science and Engineering, Michigan Technological University, Houghton, Michigan 49931, USA

†These authors contributed equally.

*Correspondence: yunhangh@mtu.edu, wangchunling@sjtu.edu.cn

1. X-ray diffraction patterns

The X-ray diffraction (XRD) patterns of Au/WO_3 and WO_3 agreed well with the standard one of monoclinic WO_3 (JCPDS Card No. 43-1035) with lattice parameters a, b, and c equal to 7.297, 7.539, and 7.688 Å, respectively. Photo-deposition of Au did not change the crystallinity of WO_3, while a weak peak at 38.337° corresponding to metallic Au appeared (JCPDS Card No. 01-1174, lattice parameter a = 4.078 Å).

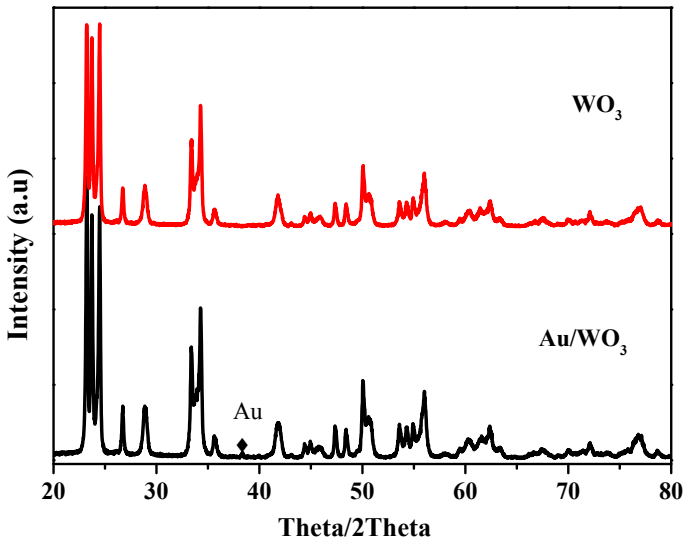

Fig. S1 XRD patterns of Au/WO_3 and WO_3.

2. Size distribution of Au nanoparticles

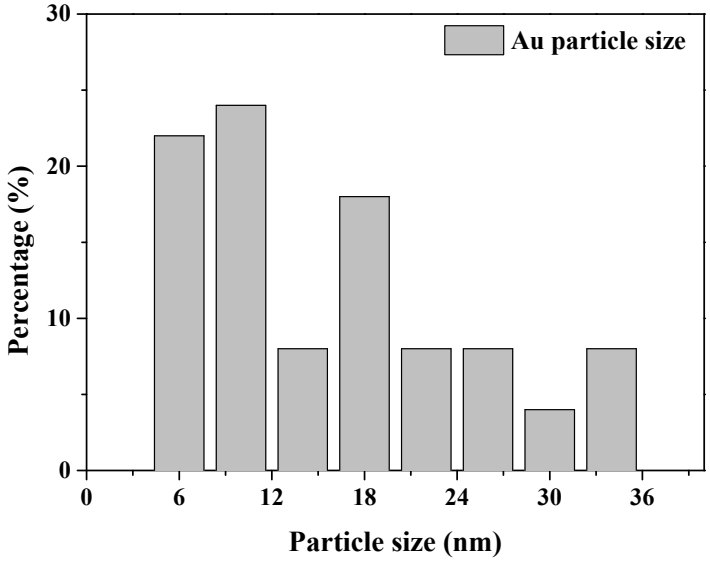

Fig. S2 Size distribution of Au nanoparticles in Au/WO_3 based on the TEM images.

3. N_2 adsorption-desorption isotherm

Approximate type V isotherms were obtained for Au/WO_3 and WO_3. The Brunauer–Emmett–Teller (BET) surface area of Au/WO_3 and WO_3 were 4.5055 and 4.1361 m^2/g, respectively. The Barrett–Joyner–Halenda (BJH) average pore diameter and volume of Au/WO_3 were 261.572 Å and 0.036819 cm^3/g, similar to those of WO_3 (263.428 Å and 0.037236 cm^3/g).

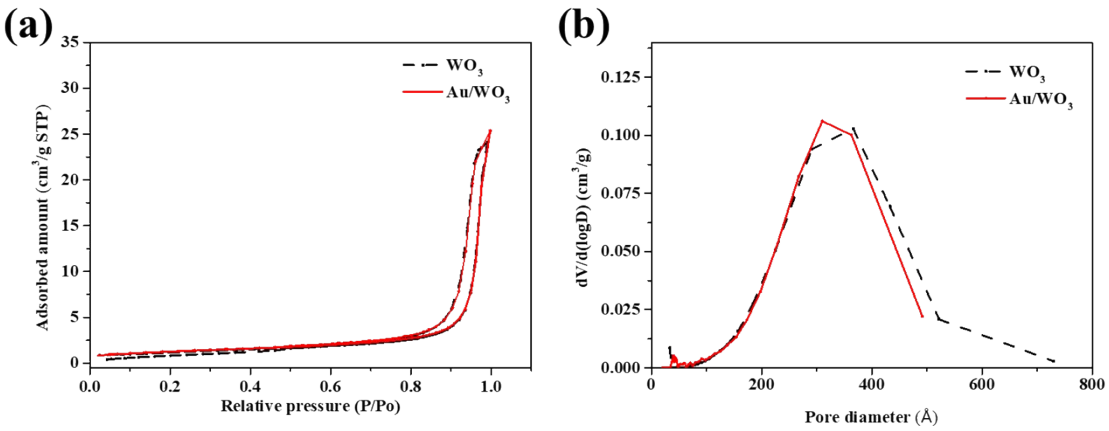

Fig. S3 Results of N_2 adsorption-desorption measurement of Au/WO_3 and WO_3. (a) N_2 adsorption-desorption curve. (b) Pore distribution curve.

4. X-ray photoelectron spectra

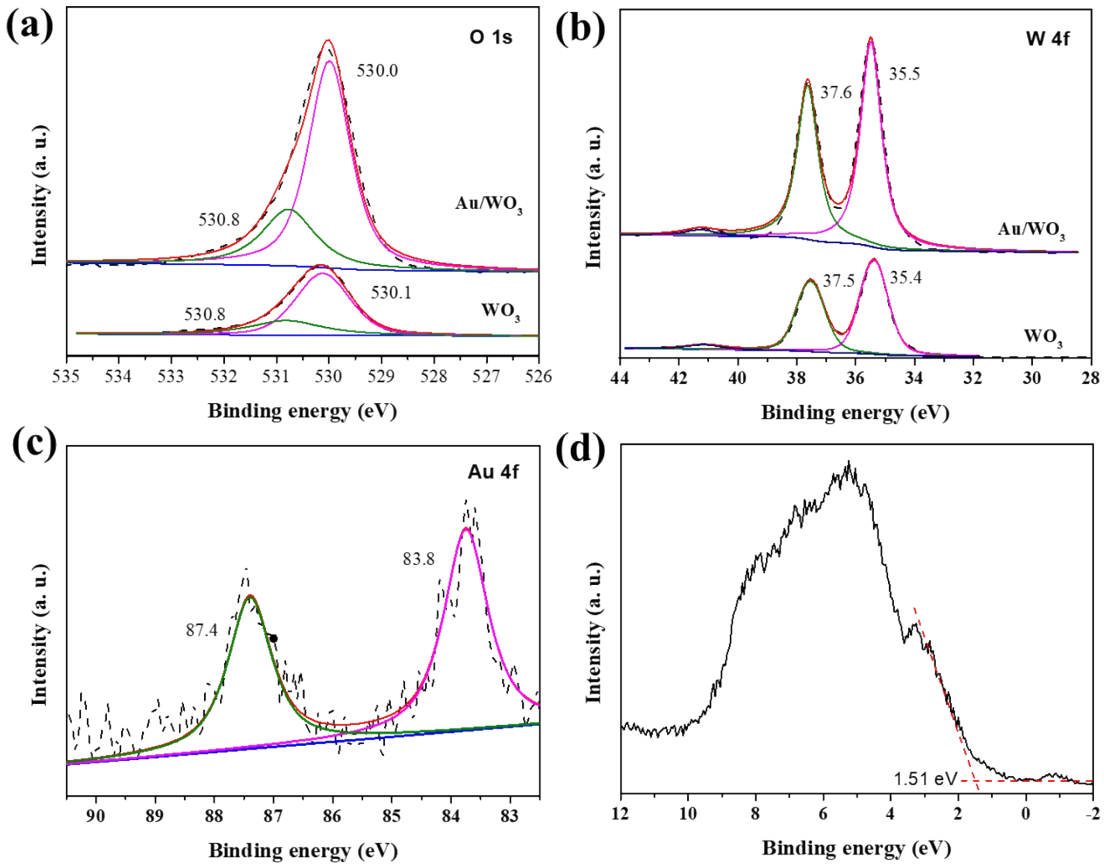

Fig. S4 XPS spectra of Au/WO_3 and WO_3. (a) O 1s XPS spectra of Au/WO_3 and WO_3. (b) W 4f XPS spectra of Au/WO_3 and WO_3. (c) Au 4f XPS spectrum of Au/WO_3. (d) valence-band XPS spectrum of Au/WO_3.

5. Mott-Schottky plot

Mott–Schottky plots for Au/WO_3 were recorded at 500, 1000, 1500, and 2000 Hz in the dark, from which the Fermi level was demonstrated as 0.71 V (vs NHE).

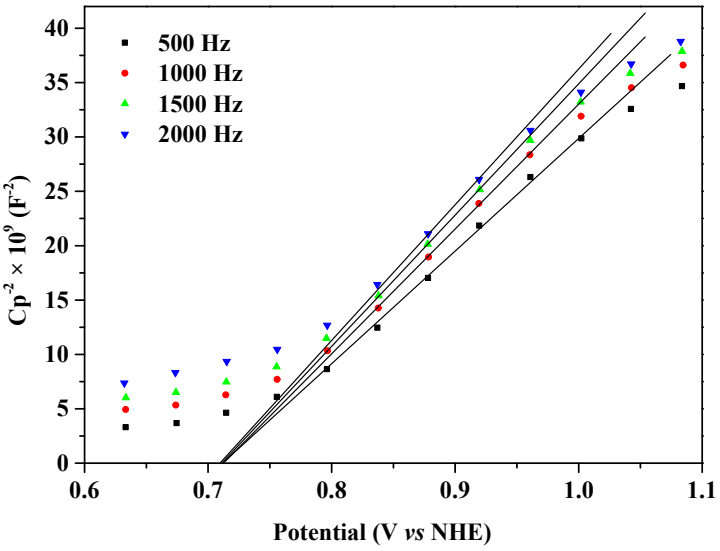

Fig. S5 Mott–Schottky plots of Au/WO_3.

6. Schematic reactor

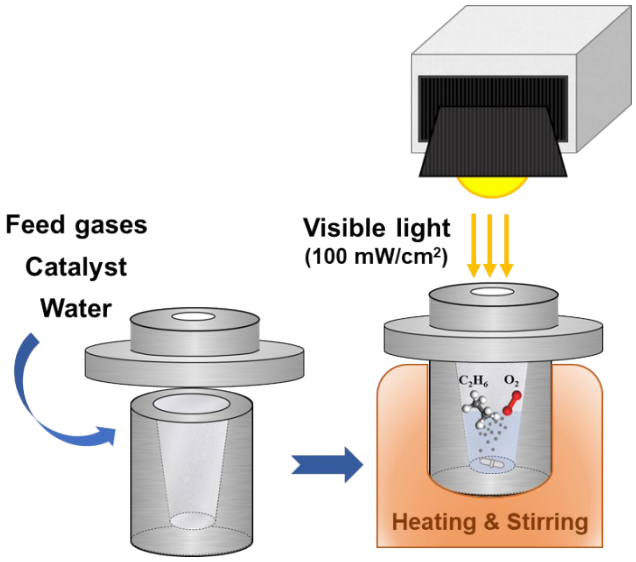

Fig. S6 Scheme of the reactor for visible-light driven photo-oxidation of ethane.

7. ^{1}H nuclear magnetic resonance spectrum

^{1}H NMR was conducted to identify the liquid products in two-hour photocatalytic reaction at 100 ºC. The signals of CH_3CH_2OOH, CH_3CH_2OH, CH_3CHO, $CH_3CH(OH)_2$, CH_3COOH, CH_3OOH, $HOCH_2OOH$, HCOOH, and dissolved C_2H_6 were observed, as referred to previous reports.[1-3] The chemical shifts of CH_3CH_2OOH were further confirmed by DFT calculations (-CH_3 at 1.21 ppm, -CH_2- at 4.18 ppm), in comparison with those of CH_3CH_2OH (-CH_3 at 1.20 ppm, -CH_2- at 3.89 ppm).

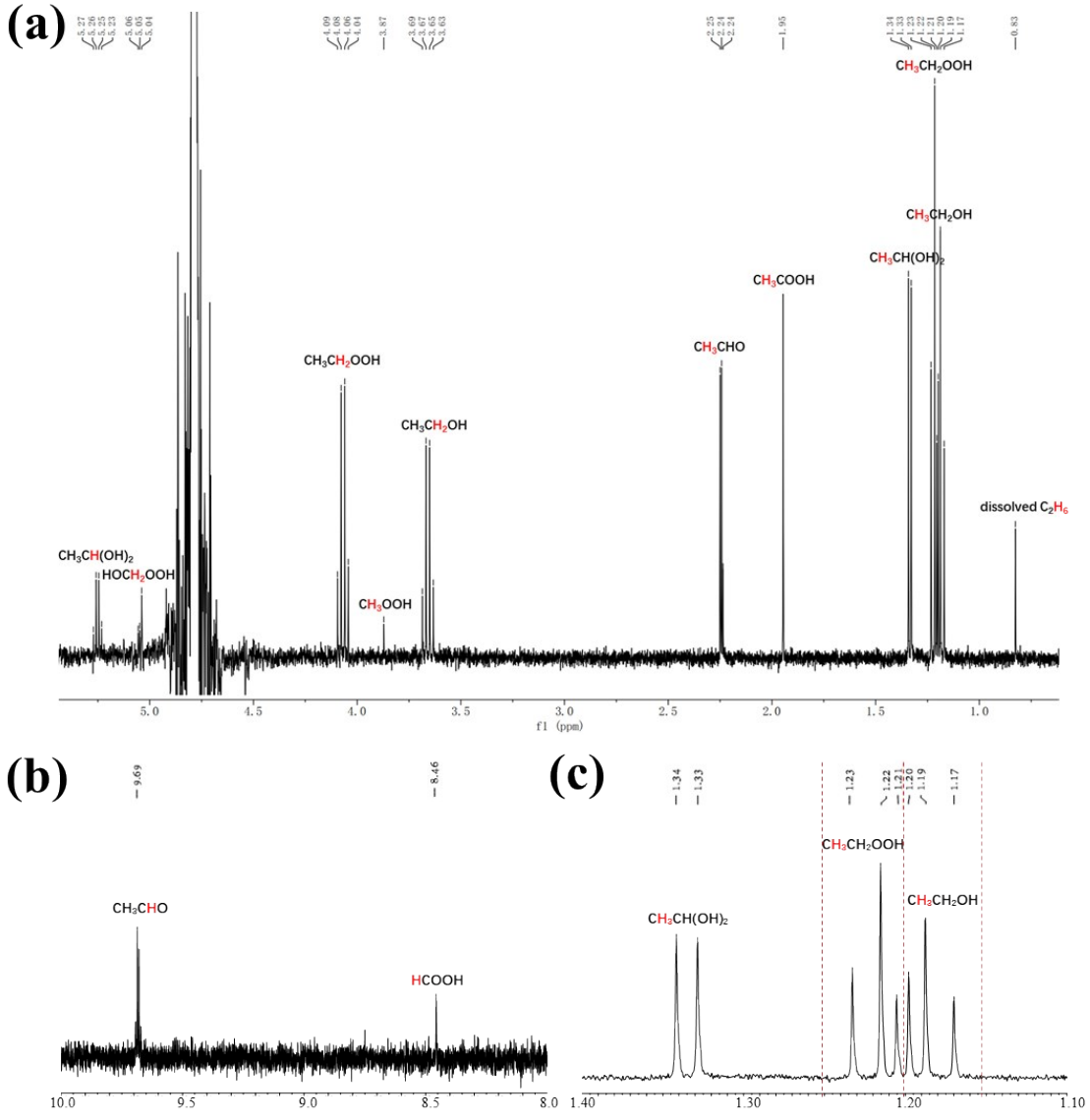

Fig. S7 ^{1}H nuclear magnetic resonance spectra of the liquid products.

8. Gas chromatography-mass spectrometry results

The liquid products generated in two-hour photocatalytic reaction over Au/WO_3 at 100 ºC in the presence of general or isotope-labeled reactants (O^{18}_2, H_2O^{18}, or D_2O) were analyzed by GC-MS. All the C2 products (CH_3CH_2OOH, CH_3CH_2OH, CH_3CHO, and CH_3COOH) were detected whose GC-MS spectra agree well the standard ones in the database while C1 products could not be clearly identified due to their tiny amounts.

Moreover, it should be noted that there should be only two origins of oxygen in the products, namely, O_2 and H_2O. The result of the O^{18}_2 experiment was analyzed combined with that of the H_2O^{18} experiment since there could be some experimental errors due to the impurity of the isotope-labelled reactants and the influence of air.

When using $O^{18}{}_2$ as the reactant, $CH_3CH_2O^{18}O^{18}H$ was detected (Fig. S8b) while the GC-MS spectrum with H_2O^{18} (Fig. S8c) is the same as that with the general reactants (Fig. S8a). This indicates that O in CH_3CH_2OOH originated from O_2 and the weak m/z signal at 62 in Fig. S8b is due to the experimental error. In addition, CH_3CH_2OOD was detected when using D_2O as the reactant (Fig. S8d).

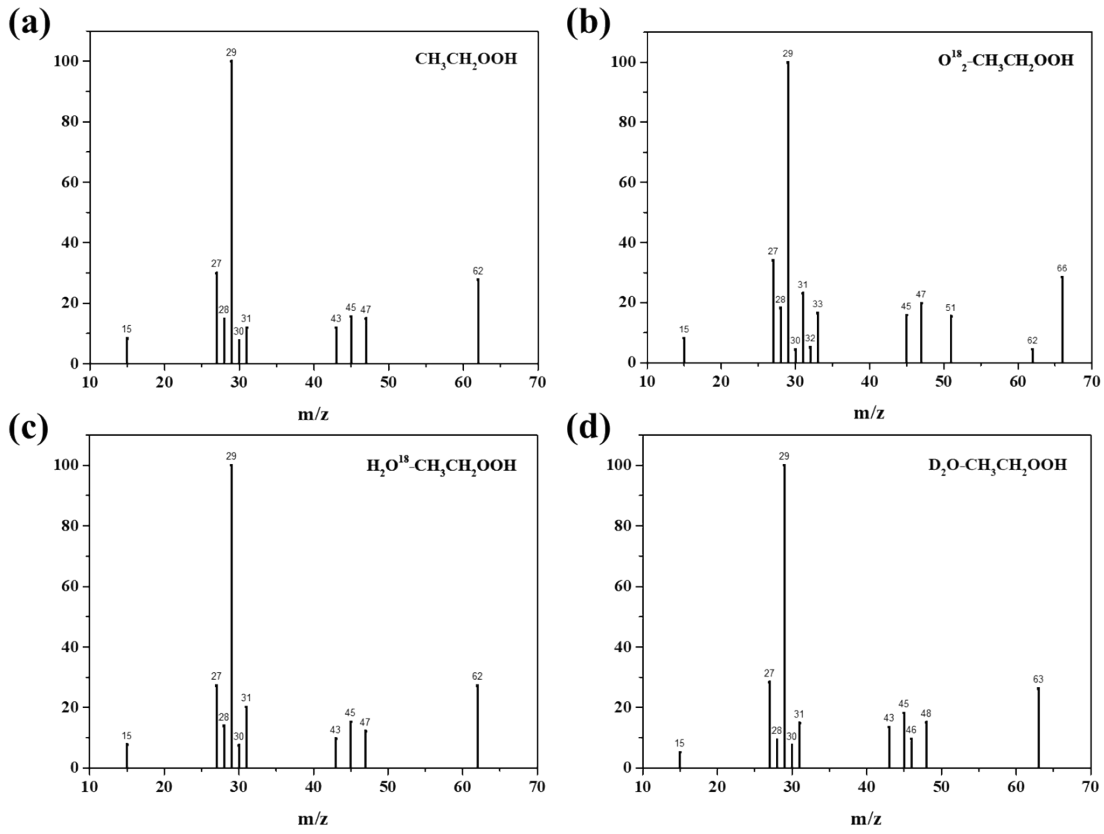

Fig. S8 GC-MS spectra for C_2H_5OOH.

Similar to the above discussion on CH_3CH_2OOH, $CH_3CH_2O^{18}H$ was detected with $O^{18}{}_2$ as the reactant (Fig. S9b) while the GC-MS spectrum with H_2O^{18} (Fig. S9c) is identical to that obtained using the general reactants (Fig. S9a). Therefore, we believe O in CH_3CH_2OH came from O_2 rather than H_2O. Moreover, D in D_2O was not detected in the produced CH_3CH_2OH (Fig. S9d).

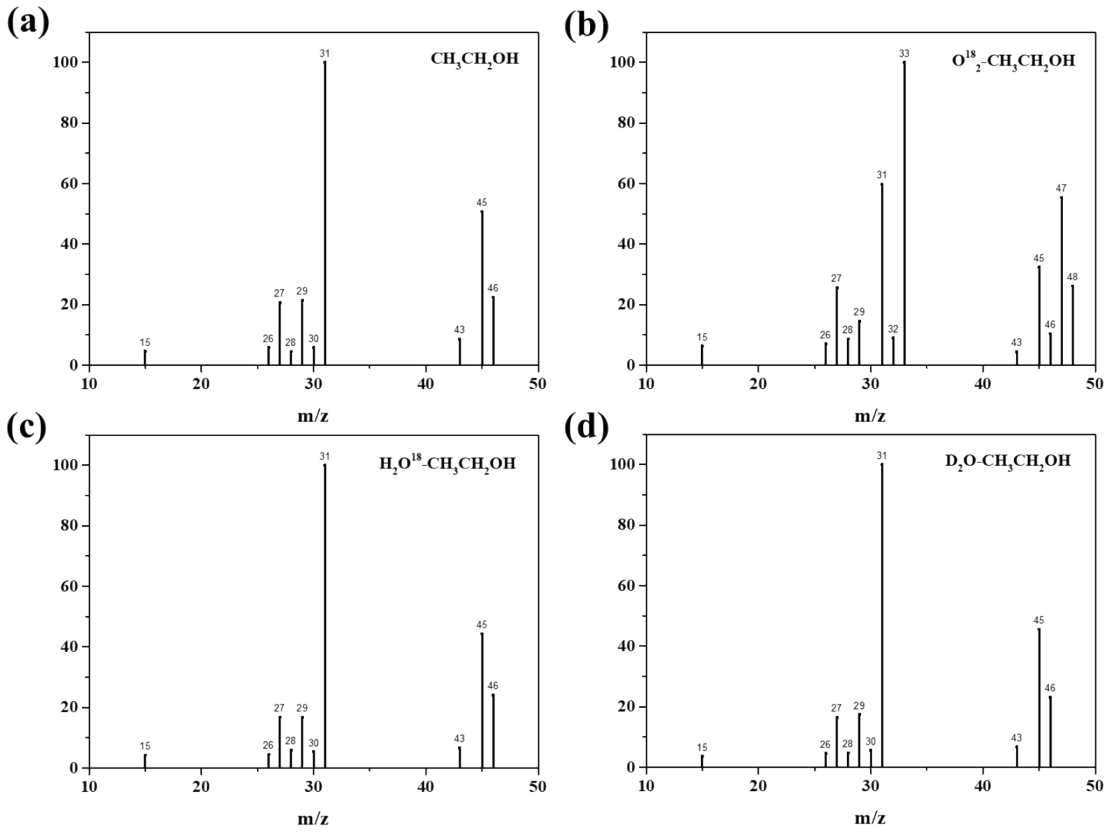

Fig. S9 GC-MS spectra for CH_3CH_2OH.

From the GC-MS spectra of the $O^{18}{}_2$ and H_2O^{18} experiments (Fig. S10 b and c), it could be seen that both O_2 and H_2O contributed to O atoms in CH_3CHO. In contrast, H in H_2O made no contribution to the generation of CH_3CHO due to the identical spectra obtained with H_2O and D_2O (Fig. S10 a and d).

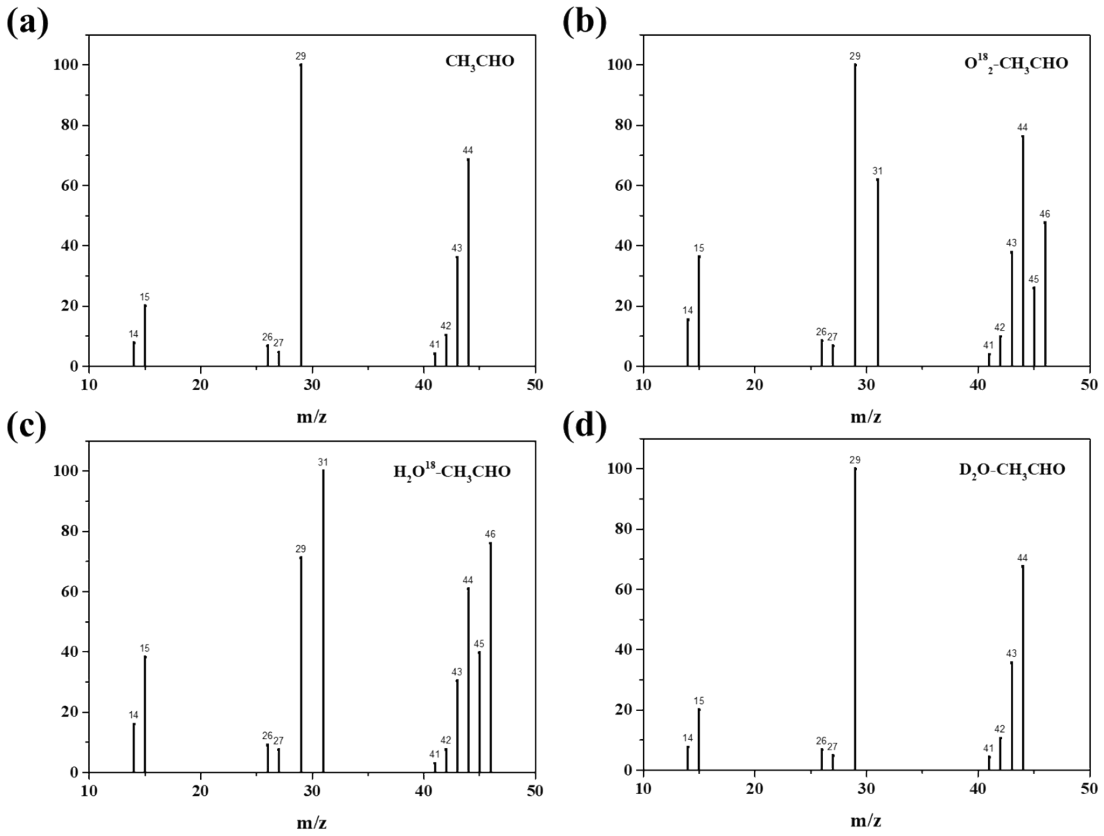

Fig. S10 GC-MS spectra for CH_3CHO.

The GC-MS spectra of the $O^{18}{}_2$ and H_2O^{18} experiments (Fig. S11 b and c) were quite similar, indicating the co-existence of CH_3COOH, $CH_3CO^{18}O^{18}H$, and $CH_3CO^{18}OH$ (or $CH_3COO^{18}H$). Thus, O atoms in CH_3COOH were derived from either O_2 or H_2O. Additionally, as revealed in Fig. S11d, H atom in the carboxy group partially originated from H_2O.

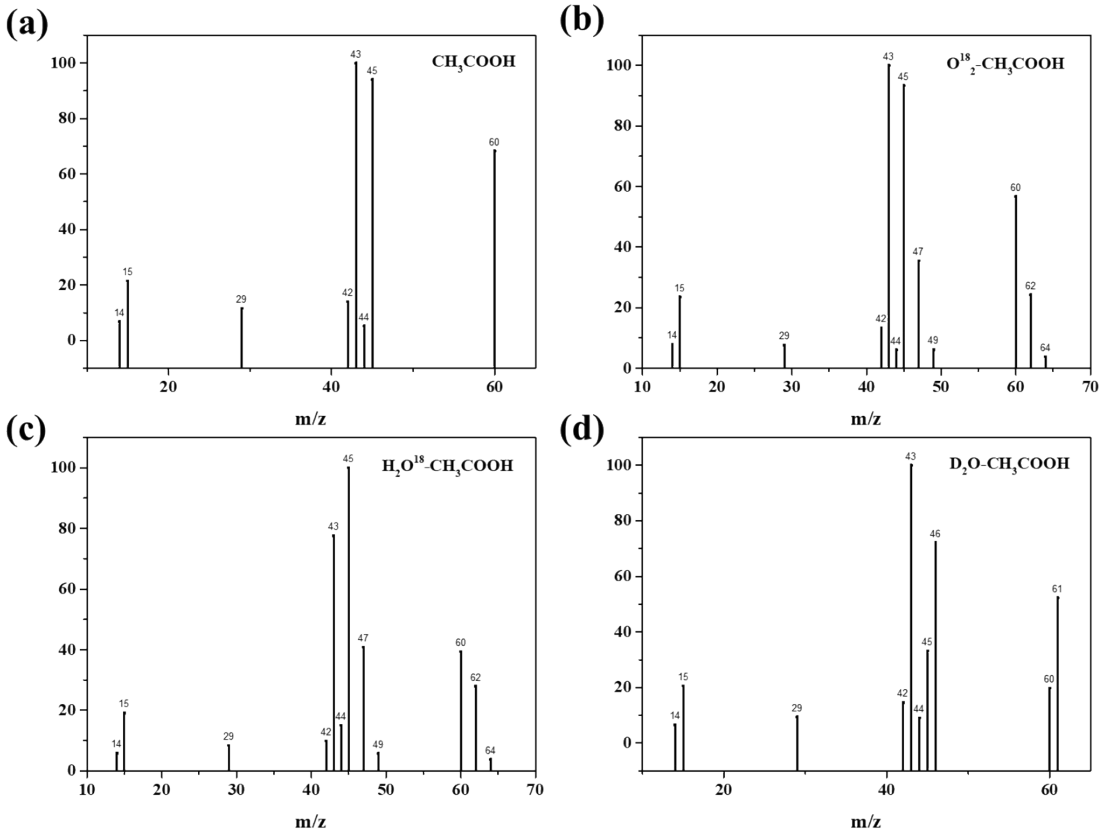

Fig. S11 GC-MS spectra for CH_3COOH.

9. Comparison of activities over various catalysts

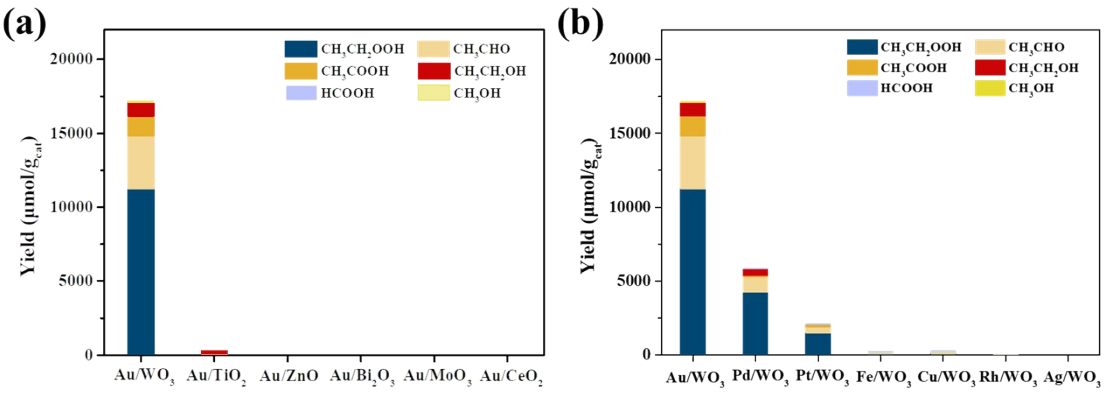

Fig. S12 Visible-light driven photocatalytic ethane oxidation over various catalysts at 100 ºC (reacting for 2 h in 20 mL water). (a) Photocatalytic ethane oxidation over Au-loaded catalysts. (b) Photocatalytic ethane oxidation over WO_3 catalysts loaded with different metals.

10. The effect of Au loading amount on the catalytic activity

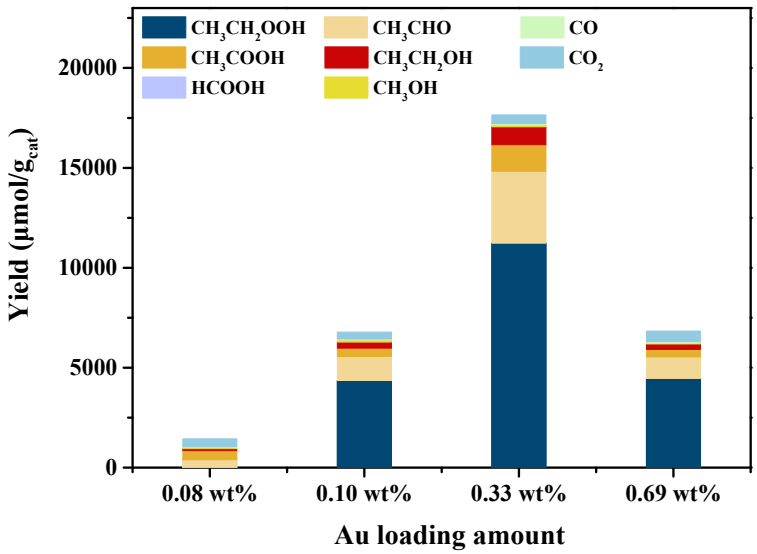

Fig. S13 Visible-light driven photocatalytic ethane oxidation over Au/WO_3 catalysts with various Au loading amounts (reacting for 2 h in 20 mL water at 100 ºC).

References

1. Jin, R., Peng, M., Li, A., Deng, Y., Jia, Z., Huang, F., Ling, Y., Yang, F., Fu, H., Xie, J., et al. (2019). Low Temperature Oxidation of Ethane to Oxygenates by Oxygen over Iridium-Cluster Catalysts. J. Am. Chem. Soc. *141*, 18921-18925.

2. Forde, M. M., Armstrong, R. D., Hammond, C., He, Q., Jenkins, R. L., Kondrat, S. A., Dimitratos, N., Lopez-Sanchez, J. A., Taylor, S. H., Willock, D., et al. (2013). Partial Oxidation of Ethane to Oxygenates Using Fe- and Cu-Containing ZSM-5. J. Am. Chem. Soc. *135*, 11087-11099.

3. Wang, S., Li, H., He, M., Cui, X., Hua, L., Li, H., Xiao, J., Yu, L., Rajan, N. P., Xie, Z., et al. (2019). Room-temperature conversion of ethane and the mechanism understanding over single iron atoms confined in graphene. J. Energ. Chem. *36*, 47-50.